

# An Automatic Guidance and Quality Assessment System for Doppler Imaging of Umbilical Artery

Chun Kit Wong<sup>1</sup>, Manxi Lin<sup>1</sup>, Alberto Raheli<sup>1</sup>, Zahra Bashir<sup>2</sup>, Morten Bo Søndergaard Svendsen<sup>2</sup>, Martin Grønnebæk Tolsgaard<sup>2</sup>, Aasa Feragen<sup>1</sup>, and Anders Nymark Christensen<sup>1</sup>

<sup>1</sup> Technical University of Denmark

<sup>2</sup> CAMES Rigshospitalet  
ckwo@dtu.dk

**Abstract.** Examination of the umbilical artery with Doppler ultrasonography is performed to investigate blood supply to the fetus through the umbilical cord, which is vital for the monitoring of fetal health. Such examination involves several steps that must be performed correctly: identifying suitable sites on the umbilical artery for the measurement, acquiring the blood flow curve in the form of a Doppler spectrum, and ensuring compliance to a set of quality standards. These steps rely heavily on the operator’s skill, and the shortage of experienced sonographers has thus created a demand for machine assistance. In this work, we propose an automatic system to fill the gap. By using a modified Faster R-CNN network, we obtain an algorithm that can suggest locations suitable for Doppler measurement. Meanwhile, we have also developed a method for assessment of the Doppler spectrum’s quality. The proposed system is validated on 657 images from a national ultrasound screening database, with results demonstrating its potential as a guidance system.

**Keywords:** Fetal Ultrasound · Umbilical Artery · Doppler Imaging

## 1 Introduction

Due to its non-invasive nature, ultrasound is widely used for routine monitoring of fetal health. In the third-trimester, ultrasound screenings are utilized to monitor potential growth restrictions of the fetus and the blood supply through the umbilical cord (UC). These screenings examine several anatomical standard planes formally defined in guidelines [2] developed by the International Society of Ultrasound in Obstetrics and Gynecology (ISUOG), which aims to ensure accurate measurement. In practice, conducting such examinations while adhering to the guidelines is technically demanding and often relies on the experience of the operators. However, due to the shortage of sonographers, third-trimester screenings are often performed by clinicians not specialized in ultrasound acquisition [3,11]. To assist these clinicians in acquiring high quality images, this paper presents an automatic system for operator guidance in assessment of the

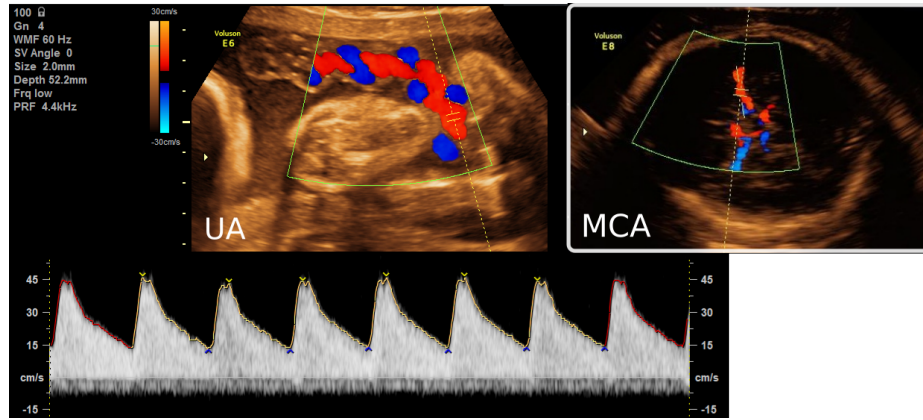


Fig. 1: Examples of two fetal standard planes in Doppler ultrasound. **Left:** Umbilical Artery (UA) including the spectral Doppler waveform. **Right:** Middle Cerebral Artery (MCA). Note how on the MCA, the vessel is running parallel to the long axis of the vessel’s segmentation, making angle estimation from segmentation straightforward. In UA, however, the vessels are usually intertwined, which means the angle cannot be trivially inferred from the segmentation.

umbilical artery (UA), which is a standard plane crucial for monitoring of the fetal blood supply, but has rarely been studied in existing works.

Examination of blood flow with ultrasound is performed over two steps: identifying and placing a measurement gate on a suitable site with color Doppler imaging, followed by measuring the blood flow curve in the form of spectral Doppler waveform with pulsed Doppler (see Fig. 1). These waveforms, which allow assessment of UA as well as the middle cerebral artery (MCA), play an important role in the third-trimester ultrasound screening [7]. A number of machine learning techniques have been used to support analysis of Doppler waveforms. Multiple works [5,9] have explored the automatic diagnosis on waveform images acquired by clinicians. Hoodbhoy et al. [5] identified fetuses at increased risk of adverse perinatal outcomes with multiple kernel learning. Naftali et al. [9] built a support vector machine, a K-nearest model, and a logistic regression model for identifying unseen UC abnormalities from the waveforms. While these studies show a clear potential for AI-based diagnosis, the studies were conducted using waveforms acquired by experienced clinicians. As noted by Necas [10], even with the availability of guidelines, mistakes are still commonly observed in practice.

Meanwhile, acquisition of an optimal Doppler waveform requires consistent, manual adjustment of various parameters, which increases the mental load on the operator [14]. This motivates research in automation of the ultrasound acquisition procedure. In this direction, MCANet [14] is developed to propose positions for measurement gate placement. In contrast to MCANet, we consider Doppler measurement at the UA, and are, to the best of our knowledge, the first to address this problem. In addition, we also introduce a study protocol for assess-

Table 1: ISUOG guidelines on using Doppler ultrasound in obstetric

Criterion	Description
Anatomical site	the Doppler signal must be measured in a free loop of the UC
Angle of insonation	the angle to the blood flow should be less than $30^\circ$ , indicating a near-vertical presentation of the blood vessel
Image clarity	the resulting Doppler signal should be clear, without artifacts, and with an accurate trace
Sweep speed	resulting Doppler signal should have 3-10 waveforms visible
Dynamic range	in the resulting Doppler signal, the waveforms should occupy more than 75% of the y-axis

ing the quality of the acquired Doppler waveforms. In summary, we contribute with **1)** an automatic detection of appropriate sites for UA Doppler measurement, while taking both location and insonation angle into account, and **2)** an automatic evaluation of the Doppler waveforms to ensure sufficient quality.

## 2 Method

We propose an image analysis pipeline that is based directly on the ISUOG guidelines (see Table 1). The first two criteria relate to the presentation of UA in the chosen ultrasound plane, whereas the remaining three criteria relate to the quality of the resulting waveforms. As such, the ISUOG criteria align well with a 2-step process. First, we assist the ultrasound operator by giving feedback on the presentation of the UA and suggesting a suitable gate location for measuring the Doppler spectrum. Next, we consider the resulting spectrum, either accepting or rejecting the combination of ultrasound plane and gate. In this way, we ensure that the examination maintains a high quality, while also giving the operator feedback on potential problems in the image acquisition.

### 2.1 Deep Learning-based Processing of Color Doppler Images

As a first step in our pipeline, we need to identify a vessel, and a gate location within the vessel. This vessel needs to be an artery (as opposed to a vein) satisfying the first two ISUOG criteria. While it might seem trivial to segment vessels that are colored red and blue and measure their angle, Fig. 1 illustrates how this problem is significantly harder for the UA, where the vessel twists and turns around itself, than it is for the MCA. We tackle this as a modified object detection problem where, instead of just detecting potential gate locations within vessels as being acceptable or not, we add a regression head to the detection algorithm in order to encode its angle (see Fig. 2).

*Modifying Faster R-CNN’s head to predict vessel angle at proposed locations.* We base our UA gate location algorithm on the Faster R-CNN object detection algorithm [12]. Faster R-CNN first generates a feature map using a backbone

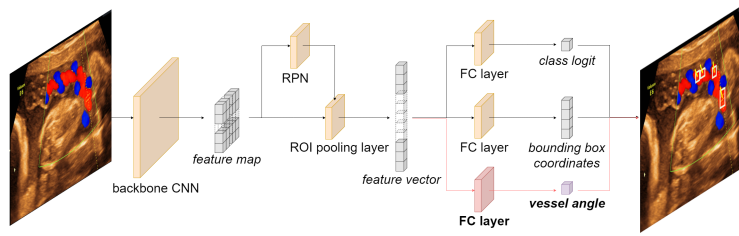


Fig. 2: Network architecture: Faster R-CNN with an extra sibling FC layer branch added for vessel angle prediction.

CNN network, which is fed to a Region Proposal Network (RPN) to propose candidate regions of interest (ROIs). Then, an ROI pooling layer is employed to extract, pool, and flatten features corresponding to the proposed ROIs, which are finally passed to two sibling branches of fully connected (FC) layers for classification and bounding box regression of the proposed ROIs. The loss function proposed in the original paper is given by:

$$L_{FasterRCNN}(\{p_i\}, \{t_i\}) = \frac{1}{N_{cls}} \sum_i L_{cls}(p_i, p_i^*) + \lambda \frac{1}{N_{reg}} \sum_i p_i^* L_{reg}(t_i, t_i^*) \quad (1)$$

where  $p_i$  is the predicted probability that the  $i$ -th proposed ROI at the predicted coordinates  $t_i$  is a valid object, with  $p_i^*$  and  $t_i^*$  as the corresponding ground-truths. The log loss  $L_{cls}$  is normalized by the batch size  $N_{cls}$ , and the smooth L<sub>1</sub> loss  $L_{reg}$  by the number of proposed ROIs  $N_{reg}$ , with  $\lambda$  balancing the terms.

In our setting, we want to detect potential gate locations that satisfy both the anatomical site and angle requirements of the ISUOG criteria. To achieve this, the standard classification branch predicts whether the anatomical site criterion is fulfilled. Then, we enrich the Faster R-CNN model with an extra sibling FC layer branch to predict the underlying vessel’s angle at each proposed ROI.

To train this modified model, we included another term in Eq. 1 to regress the predicted angle against ground truth annotations (see Fig. 4a):

$$L(\{p_i\}, \{t_i\}, \{a_i\}) = L_{FasterRCNN}(\{p_i\}, \{t_i\}) + \mu \frac{1}{N_{reg}} \sum_i p_i^* L_{reg}(a_i, a_i^*) \quad (2)$$

where  $a_i$  and  $a_i^*$  are the predicted and ground truth angle of the  $i$ -th proposed ROI, and  $\mu$  is another balancing factor.  $\lambda$  and  $\mu$  are set to 1 and 10, respectively.

*Locating source of ultrasound beam.* The vessel angle estimated using our modified Faster-RCNN network indicates the vessel’s direction (see Fig. 4b). However, the angle of insonation needed to assess the second ISUOG criterion refers to the angle of the vessel with respect to the direction of the ultrasound beam. Hence, to assess whether the angle is acceptable and give suitable feedback to the operator, we need to determine the direction of the ultrasound beam and use it to calibrate the angle prediction from the network.

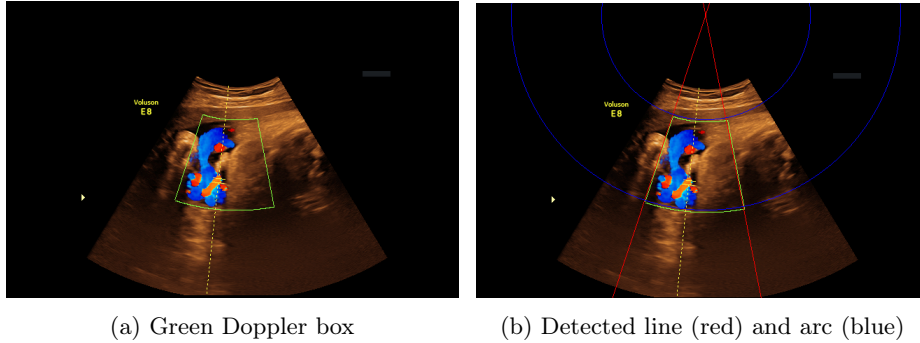


Fig. 3: Locating source of the ultrasound beam by using the green Doppler box.

We begin with determining the direction of the ultrasound beam by utilizing the green Doppler box, which becomes active during color Doppler acquisition (see Fig. 3a). A binary mask of the green Doppler box is first obtained by color thresholding on the RGB pixels, followed by enhancing the mask using a watershed transform [6]. Next, a Hough line detection algorithm [1] is used to identify the two radial line segments on each side of the box. The ultrasound source is located at the intersection between the two line segments. As an extra step to prevent erroneous detection, we verify that we are able to detect the two arc lines with Hough circle detection when the center location is constrained to be at the intersection point from the previous two Hough lines (see Fig. 3b).

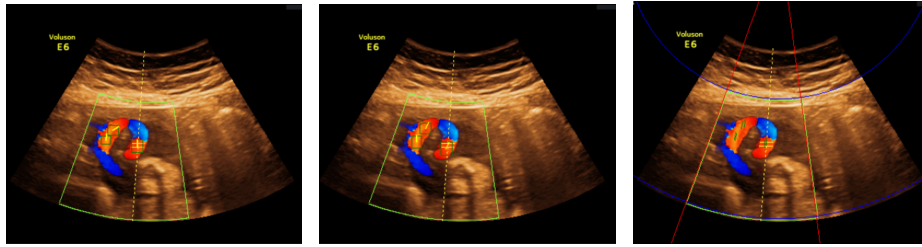
*Determining the angle of insonation.* Next, from the identified location of the ultrasound source, it is straightforward to compute a vector map pointing at the direction of the ultrasound source from each pixel (see Fig. 4c). By expressing the vessel angle predicted by the network as another vector, the angle of insonation can be easily calculated using the law of cosine.

Based on the above, we obtain a detection algorithm that proposes, to the operator, gate locations fulfilling both anatomical and angle requirements. This algorithm is developed using images acquired with different models of GE scanners. Adjustments for cross-vendor applications is likely necessary, but we expect the method to work equally well, since it is a convention in Doppler ultrasound to use variations of red and blue while encoding flow directions [2].

## 2.2 Processing of Pulsed Doppler Spectrum Images

From the suggested gate locations (see Sec. 2.1), an operator could choose the best one for spectrum acquisition with pulsed Doppler. Next, we present our processing to assess the quality of the resulting spectrum.

*Segmentation of the Doppler Spectrum.* Prior to analyzing the Doppler spectrum, all irrelevant visual confounders, such as tracing lines indicating measurements



(a) Expert annotated boxes and tangential lines (b) Model predicted boxes and tangential lines (c) Vectors pointing in direction of ultrasound source

Fig. 4: Different stages in processing Color Doppler image.

made by the scanner (see Fig. 1), are first removed from the image to prevent bias in our method. Since the confounders are all colored, they can be delineated from the grey spectrum by identifying pixels with large variance across the color (i.e. RGB) channel, and removed by inpainting with biharmonic functions.

Next, the spectrum is segmented using a random walk segmentation algorithm [4], as watershed is found to be insufficient. From the mask of the segmented spectrum, the envelope of the spectrum can be identified from the boundary. Then, the  $x$ -axis line of the spectrum is detected using the Hough line detection algorithm, and used to remove anything below and fill any holes above.

*Identification of Individual Waveforms.* From the spectrum segmentation, peaks and valleys are detected along the upper envelope. To avoid over-detection, the envelope is Gaussian-smoothed prior to running the detection algorithm. Besides that, the detected peaks (and valleys) are forced to have a minimum distance of 70 pixels between each other. Individual waveforms are then identified with the rule that a complete waveform starts and ends at valleys with a peak in between.

*Determining Waveform Properties.* Having identified individual waveforms, we need to quantify their quality in order to assess whether the waveform as a whole satisfies the last three ISUOG criteria. To obtain this, the spectrum image pixels are first rescaled to floating point values between 0 and 1. Using the spectrum segmentation, we mask out the relevant part of the spectrum to compute the mean intensity of pixels in each individual waveform. Two threshold values are defined to classify the waveform as having good, moderate, or poor clarity (see Fig. 5). In our experiment, these thresholds are set empirically to 0.56 and 0.36. Heights of the waveform are determined from the peak coordinate and the  $x$ -axis line, followed by expressing them as a percentage of the positive  $y$ -axis.

### 3 Dataset

The data used for this study were gathered under permission (ANONYMOUS) from a national screening database containing images acquired between 2009

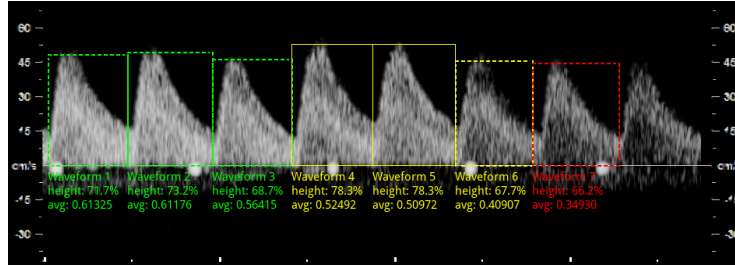


Fig. 5: Waveform clarity and height. Good clarity is indicated in green (mean intensity  $> 0.56$ ), moderate in yellow, and poor in red (mean intensity  $< 0.36$ ) is poor. Dotted line indicates waveforms with height less than 75%.

and 2019 as part of the standard prenatal care. In total, 657 DICOM images of Doppler ultrasound examination at the UA were retrieved from the database. From each image, two regions were cropped and exported separately: (1) the b-mode ultrasound image with color Doppler overlays (for simplicity, we will call this the color Doppler image), and (2) the pulsed Doppler spectrum image.

Subsequently, the color Doppler images were annotated by a clinician using the open-source tool LabelMe [13]. On each image, regions corresponding to the correct anatomical site (i.e. the UA) were annotated with bounding box, which was done sparsely due to the inherent difficulty in annotating all correct anatomical sites with just bounding boxes. Finally, a tangential line going in the direction of the blood vessel were added on top of each annotated bounding box to indicate the vessel’s angle (see Fig. 4a).

## 4 Experiments and Results

### 4.1 Experimental Settings

The modified Faster R-CNN model was implemented in PyTorch 1.13.1 on an AlmaLinux 8.7 system. The model backbone is a ResNet50 FPN pre-trained on COCO [8] and fine-tuned on our annotated images at 80:20 train-test split with SGD optimizer, which converged after 20 epochs. The learning rate was 0.005 at the first epoch and reduced 0.1 times every 3 epochs. The batch size was set to 2. This training took less than 1 hour on an NVIDIA RTX A6000 GPU. The experiments on waveform quality assessment were conducted on a server (CPU: EPYC 7252 8-Core Processor; RAM: 32GB), using image processing algorithms implemented in Scipy 1.10.0 and Scikit-Image 0.19.3.

### 4.2 Results

*Automatic gate placement.* The ground-truth gate locations in our dataset are under-annotated (see Sec. 3). Hence, to better estimate the error in our angle

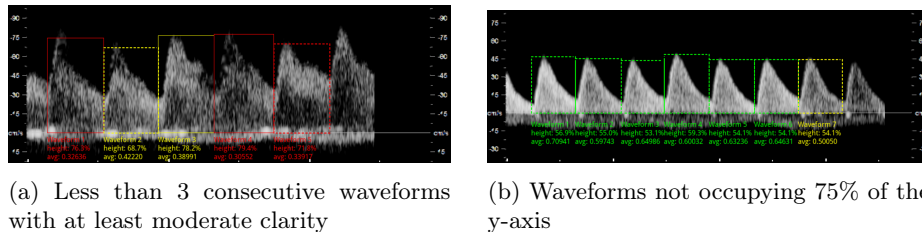


Fig. 6: Example spectrums not meeting the ISUOG criteria. Zoom in for details.

prediction, we compared each model-suggested gate position box with the closest ground truth box, matched according to the Euclidean distance between the centroid of the two boxes. Pairs separated with a too-far distance (greater than 10 pixels; see Appendix 1) were excluded from this analysis. With a 5-fold cross validation, 85.37% (std 2.97%) of the ground truth has a matched prediction, with a mean absolute error of  $19.36^\circ$  (std  $0.47^\circ$ ) in angle prediction.

Additionally, an experienced clinician was engaged to check through the model predictions on 737 test images and reject images with at least one unacceptable box prediction, giving a conservative performance estimate. This gave an acceptance rate of 68.1%.

*Waveform quality assessment.* We applied the proposed waveform quality assessment pipeline on the 657 spectrum images. Fig. 6 presents two images that has failed to meet the ISUOG waveform clarity and dynamic range criteria, identified by our method. This demonstrates the promising potential of our pipeline being alternatively deployed as a retrospective waveform quality assessment tool.

## 5 Discussion and Conclusion

We attempted to address a real clinical problem in this paper: providing guidance to an operator on the Doppler assessment of UA, which is significant due to the shortage of skilled sonographers. We proposed a method for guiding the operator on where to place the measurement gate, which has shown promising performance on our test data. Furthermore, another method was proposed to assess the quality of the acquired spectrum, designed to be well-aligned to the criteria specified in the ISUOG guidelines. This provides a comprehensive assessment of the scan quality, ensuring compliance to criteria such as "sweep speed" and "dynamic range", which often get neglected in actual clinical practice.

In the future, we aim to extend the method for processing live video stream directly. While new challenges is foreseen with the incorporation of temporal information, better performance can be expected in multiple ways, such as an improved accuracy in differentiating between the pulsating artery and the non-pulsating vein. Overall, we have demonstrated the potential of our method in resolving the clinical problem that has motivated its development.

## References

1. Aggarwal, N., Karl, W.C.: Line detection in images through regularized hough transform. *IEEE transactions on image processing* **15**(3), 582–591 (2006)
2. Bhide, A., Acharya, G., Bilardo, C., Brezinka, C., Cafici, D., Hernandez-Andrade, E., Kalache, K., Kingdom, J., Kiserud, T., Lee, W., et al.: Isuog practice guidelines: use of doppler ultrasonography in obstetrics. *Ultrasound in obstetrics & gynecology: the official journal of the International Society of Ultrasound in Obstetrics and Gynecology* **41**(2), 233–239 (2013)
3. Edvardsson, K., Ntaganira, J., Åhman, A., Sengoma, J.P.S., Small, R., Mogren, I.: Physicians’ experiences and views on the role of obstetric ultrasound in rural and urban rwanda: a qualitative study. *Tropical Medicine & International Health* **21**(7), 895–906 (2016)
4. Grady, L.: Random walks for image segmentation. *IEEE Transactions on Pattern Analysis and Machine Intelligence* **28**(11), 1768–1783 (2006). <https://doi.org/10.1109/TPAMI.2006.233>
5. Hoodbhoy, Z., Hasan, B., Jehan, F., Bijmens, B., Chowdhury, D.: Machine learning from fetal flow waveforms to predict adverse perinatal outcomes: a study protocol. *Gates open research* **2** (2018)
6. Huang, Y.L., Chen, D.R.: Watershed segmentation for breast tumor in 2-d sonography. *Ultrasound in medicine & biology* **30**(5), 625–632 (2004)
7. Kennedy, A.M., Woodward, P.J.: A radiologist’s guide to the performance and interpretation of obstetric doppler us. *Radiographics* **39**(3), 893–910 (2019)
8. Lin, T.Y., Maire, M., Belongie, S., Hays, J., Perona, P., Ramanan, D., Dollár, P., Zitnick, C.L.: Microsoft coco: Common objects in context. In: *Computer Vision–ECCV 2014: 13th European Conference, Zurich, Switzerland, September 6–12, 2014, Proceedings, Part V 13*. pp. 740–755. Springer (2014)
9. Naftali, S., Ashkenazi, Y.N., Ratnovsky, A.: A novel approach based on machine learning analysis of flow velocity waveforms to identify unseen abnormalities of the umbilical cord. *Placenta* **127**, 20–28 (2022)
10. Necas, M.: Obstetric doppler ultrasound: Are we performing it correctly? *Australasian Journal of Ultrasound in Medicine* **19**(1), 6 (2016)
11. Recker, F., Weber, E., Strizek, B., Gembruch, U., Westerway, S.C., Dietrich, C.F.: Point-of-care ultrasound in obstetrics and gynecology. *Archives of Gynecology and Obstetrics* **303**, 871–876 (2021)
12. Ren, S., He, K., Girshick, R., Sun, J.: Faster r-cnn: Towards real-time object detection with region proposal networks. *Advances in neural information processing systems* **28** (2015)
13. Wada, K.: labelme: Image polygonal annotation with python. <https://github.com/wkentaro/labelme> (2018)
14. Wang, S., Hua, Y., Cao, Y., Song, T., Xue, Z., Gong, X., Wang, G., Ma, R., Guan, H.: Deep learning based fetal middle cerebral artery segmentation in large-scale ultrasound images. In: *2018 IEEE International Conference on Bioinformatics and Biomedicine (BIBM)*. pp. 532–539. IEEE (2018)

## Appendix 1 Evaluating Model’s Performance

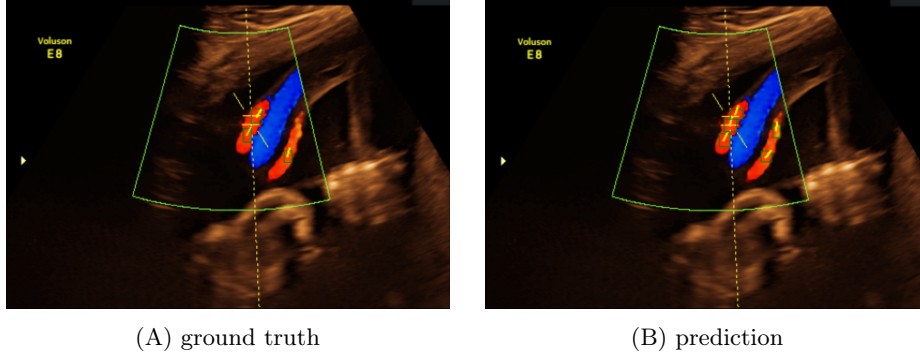


Fig. I: Manually-annotated (A) versus model-predicted (B) bounding boxes and angles. The correct anatomical sites are sparsely annotated due to laborious nature of the task, which means not every correct anatomical sites are annotated in our ground truth dataset.

Since the correct anatomical sites are under-annotated in our dataset (see Fig. I), we are unable to determine the false-positive in our predictions and, subsequently, the precision of our model. Hence, we chose to evaluate our model performance with a sensitivity-based approach. For every ground-truth box (see Fig. IA), we identify the corresponding nearest predicted box (see Fig. IB) by determining box pair that yields the shortest Euclidean distance:

$$f(\mathbf{t}_i^*) = \mathbf{t}_{\tilde{j}}, \quad \tilde{j} = \underset{j}{\operatorname{argmin}} \|\mathbf{t}_i^* - \mathbf{t}_j\|_2$$

where  $\mathbf{t}_i^*$  represents centroid of the  $i$ -th ground-truth box,  $\mathbf{t}_j$  centroid of the  $j$ -th predicted box,  $\tilde{j}$  the index of the nearest predicted box, and  $f$  the mapping function. Then, for a given threshold  $n$ , we say the ground truth box is successfully detected if its nearest predicted box is less  $n$  pixels away:

$$T := \{ \mathbf{t}_i^* \}$$

$$\tilde{T} := \begin{cases} \{ \mathbf{t}_i^* \mid \|\mathbf{t}_i^* - \mathbf{t}_{\tilde{j}}\|_2 < n \}, & \text{if } \{ \mathbf{t}_j \} \neq \emptyset \\ \emptyset, & \text{otherwise} \end{cases}$$

Finally, the sensitivity of our model is derived by calculating the percentage of successfully detected ground truth box:

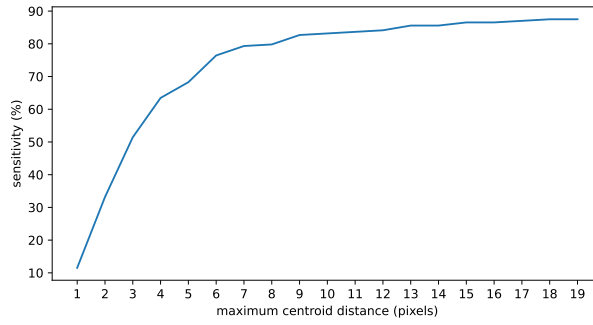
$$\text{sensitivity} = \frac{|\tilde{T}|}{|T|} \times 100\%$$

while the inaccuracy in angle prediction is estimated using the mean  $L_1$  distance between the ground truth angles  $\{a_i^*\}$  and the predicted angles  $\{a_j\}$ :

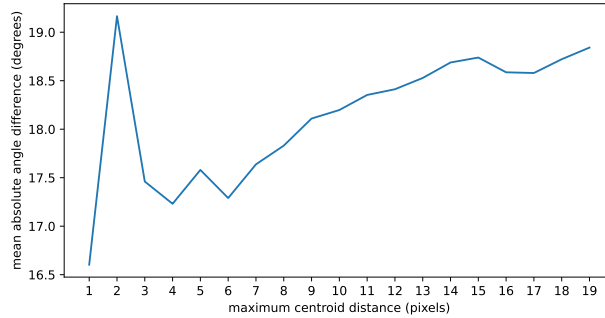
$$\Delta A = \{\|a_i^* - a_j\|\}$$

$$\bar{L}_1 = \frac{\sum \Delta A}{|\Delta A|}$$

As expected, both the sensitivity and the angle inaccuracy increased with a larger threshold  $n$  (see Fig. II). Since a higher sensitivity and lower angle inaccuracy is desired, we reported the values with  $n$  fixed to 10 (see Sec. 4.2 of the main article) to avoid over-glorifying our model in either of the two performance metrics.



(A) *sensitivity* against  $n$  (the higher the better)



(B)  $\bar{L}_1$  against  $n$  (the lower the better)

Fig. II: Evaluation of model's performance